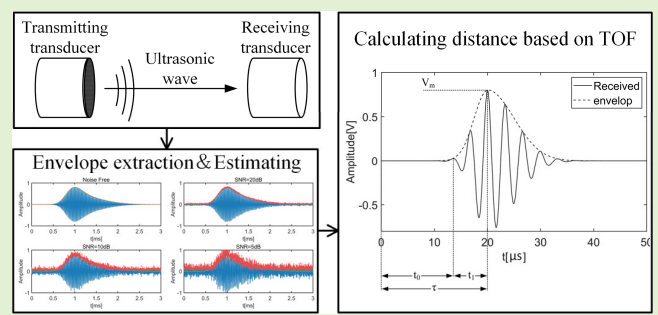


Enhancing Ultrasonic Time-of-Flight Estimation Using Adaptive Differential Evolution and Levenberg–Marquardt Algorithm

Jinglin Xiong^{ID}, Peng Mao, and Xisheng Li

Abstract—A parameter estimation algorithm based on an asymmetric Gaussian model (ACGM) is proposed to address the problems of low accuracy and susceptibility to noise in the traditional ultrasonic time-of-flight (TOF) estimation method, which improves the accuracy of TOF estimation and is less affected by noise. The algorithm is a combination of adaptive differential evolution (DE) and Levenberg–Marquardt (LM), using the DE algorithm as a global search strategy and the LM algorithm as a local search strategy. First, the received echo signal is processed using the Hilbert transform to extract the envelope, reducing dimensionality, and computational burden. Then, the adaptive DE algorithm converges quickly to a better solution, and then, the result of the adaptive DE algorithm is used as the initial value of the LM algorithm to further improve the accuracy, which solves the problem that the LM algorithm needs a good initial value to provide an accurate output. Finally, the model parameters are used to derive an accurate echo leading edge arrival time. The proposed algorithm is compared with several well-known DE variants as well as the latest algorithm in numerical simulations and ranging experiments. The results demonstrate the excellent performance of the adaptive differential evolution (ADE)–LM algorithm in the estimation of ultrasonic TOF.

Index Terms—Adaptive differential evolution (ADE), asymmetric Gaussian model, Levenberg–Marquardt (LM), ultrasonic time-of-flight (TOF).



I. INTRODUCTION

ULTRASONIC measurement plays a significant role in various applications, including flaw detection [1], [2], [3], [4], positioning [5], flow measurement [6], [7], [8], biomedical applications [9], [10], and distance measurement [11], [12], [13]. Among the large number of existing ultrasonic ranging techniques, time-of-flight (TOF) measurement stands out as a primary approach employed in ultrasonic ranging systems. TOF refers to the duration between the emission of a pulse and the reception of the reflected echo from the target. In many cases, the prevailing method for signal identification in ultrasonic systems relies on threshold level detection, which discerns the presence of a signal based on its amplitude exceeding a predetermined minimum voltage level.

Manuscript received 8 October 2023; revised 10 October 2023; accepted 10 October 2023. Date of publication 19 October 2023; date of current version 12 January 2024. This work was supported by the National Key Research and Development Program of China under Grant 2022YFC2403703. The associate editor coordinating the review of this article and approving it for publication was Dr. Wensong Wang. (*Corresponding author: Xisheng Li*)

The authors are with the School of Automation and Electronic Engineering, University of Science and Technology Beijing, Beijing 100083, China (e-mail: m202120662@xs.ustb.edu.cn; lxs@ustb.edu.cn).

Digital Object Identifier 10.1109/JSEN.2023.3324502

Nevertheless, this method becomes more vulnerable to the influence of noise. Moreover, the accuracy of direct voltage comparators lacking an analog-to-digital converter is notably suboptimal, resulting in TOF measurements that are merely half the wavelength [14], [15].

Multiple signal processing techniques have been developed with the aim of enhancing the accuracy of TOF measurements and improving the precision of ultrasound-based measurements. Impedance matching network design is widely used in ultrasonic transducer circuits to improve transducer efficiency and sensitivity while reducing signal distortion [3], [4], [16], [17]. The dual-threshold method represents a notable advancement over the traditional threshold approach [18]. Extensive research endeavors have been dedicated to exploring this area, with the overarching goal of bolstering immunity to interference, refining measurement accuracy, and expanding its applicability to diverse domains [19]. A more precise and appropriate technique for TOF estimation emerges in the form of cross correlation. This method involves cross-correlating the received signal with a reference signal, subsequently determining the TOF by identifying the maximum value in the resulting cross-correlation function [20].

Another method used for TOF estimation involves the utilization of curve-fitting methods based on models of received ultrasonic pulses. This method exhibits a remarkable capability to accurately determine TOF even under low signal-to-noise ratio conditions. Gaussian and exponential models are frequently employed in estimating TOF through curve fitting [21], [22]. In comparison to the threshold and cross-correlation methods, the model-based estimation approach offers a broader range of applications. This includes accommodating various types of ultrasonic transducers and operating effectively under low signal-to-noise ratio scenarios, thus ensuring more stable outputs.

After establishing the echo model, the estimation of parameters is transformed into a least-square problem, and the selection of an appropriate optimization algorithm allows for obtaining the desired parameters with higher accuracy. The classical least squares algorithms include the gradient descent, the Gauss–Newton method, and Levenberg–Marquardt (LM). However, the gradient descent method tends to fall into the local optimum, the Gauss–Newton fails to converge in the presence of singular matrices, and the LM heavily relies on the quality of initial values. To solve the problem of initial values for estimating, global optimization algorithms, such as particle swarm optimization (PSO) and genetic algorithms, are widely used [23]. Nonetheless, it is imperative to acknowledge that such algorithms also have some nonnegligible problems. One prominent problem is that they need a considerable number of iterations to converge to the optimum, which cannot satisfy the real-time application scenarios such as ultrasonic ranging. Meanwhile, it is often challenging to ensure the approximate stability and accuracy of the results within a limited number of iterations.

Considering the above issues, this article proposes a combination of adaptive differential evolution (ADE) and the LM algorithm for estimating ultrasonic TOF based on the asymmetric Gaussian model (ACGM). The adaptive differential evolution (DE) algorithm with excellent global search capability is used to obtain an approximation closer to the optimal solution, which is used as the initial value of the LM algorithm to converge to the optimum with only a small number of iterations. Consequently, this algorithm facilitates the attainment of more precise parameter values within a limited time.

II. ULTRASONIC SIGNAL MATHEMATICAL MODEL

Based on the ultrasonic transducer pulse-echo signal, the amplitude spectrum of the transducer pulse-echo signal can be modeled as a Gaussian spectrum centered at the transducer center frequency and having the same bandwidth as the transducer [24]

$$s(\theta', t) = \beta e^{-\alpha(t-\tau)^2} \cos(2\pi f_c(t - \tau) + \phi) \quad (1)$$

where $\theta' = [\beta, \alpha, \tau, f_0, \phi]$, α is the bandwidth, τ is the arrival time, f_c is the center frequency, ϕ is the phase, and β is the amplitude factor.

Due to the symmetric nature of the model, it cannot adequately fit real ultrasound signals that possess asymmetric envelopes. Therefore, an ACGM is proposed [25]. The echo is represented by a combination of the envelope line and linear

frequency-modulated sinusoidal components, allowing for the discrete representation of ultrasonic echoes

$$s(t) = \text{env} \cdot \cos\{2\pi f_c(t - \tau) + \psi(t - \tau)^2 + \phi\} \quad (2)$$

$$\text{env}(t, \theta) = \beta \exp(-\alpha(1 - r \tanh(m(t - \tau)))(t - \tau)^2) \quad (3)$$

where $\theta = [\beta, \alpha, r, m, \tau]$, ψ is the linear modulation frequency, ϕ is the model phase, α is the decay rate (bandwidth factor), r is the coefficient controlling the envelope asymmetry, and $\tanh(mt)$ is the hyperbolic tangent function of order m , where m is a positive integer, e.g., 16. This function is a smooth approximation of the symbolic function responsible for varying the parameter r in the very short period of time $[-\varepsilon, \varepsilon]$. Thus, the envelope signal closely resembles a Gaussian profile, characterized by two distinct decay rates before and after the peak. These two decay rates are defined as follows:

$$\begin{aligned} \text{env}(t) &= \beta \exp(-\alpha(1 - r)t^2), & t > \varepsilon \\ \text{env}(t) &= \beta \exp(-\alpha(1 + r)t^2), & t < -\varepsilon. \end{aligned} \quad (4)$$

To ensure that the above function is a valid echo envelope with a finite duration the following conditions should hold:

$$\begin{aligned} a &> 0 \\ -1 &< r < 1. \end{aligned} \quad (5)$$

The envelope has two different decay rates α_L and α_R , before and after the reference point τ

$$\alpha_L = \alpha(1 + r), \quad \alpha_R = \alpha(1 - r) \quad (6)$$

$$r = \frac{\alpha_L - \alpha_R}{\alpha_L + \alpha_R}. \quad (7)$$

To illustrate the difference between the Gaussian model and two ACGMs with different decay rates, assume that $\theta' = [1, 0.8, 1, 5, 1]$ and $\theta = [1, 1, 0.6, 16, 1.5]$, here $\psi = 1$, the center frequency is consistent with the Gaussian model as 5 MHz, the bandwidth factor unit is MHz², and the arrival time unit is μs . This is shown in Fig. 1.

III. ULTRASONIC SIGNAL PARAMETERS ESTIMATION ALGORITHMS

The received continuous waveform with noise is written as follows:

$$x(t) = s(\theta, t) + w(t) \quad (8)$$

where $s(\theta, t)$ is the ACGM, whose discrete version can be written as follows:

$$\begin{aligned} s(t_n) &= \text{env} \cdot \cos\{2\pi f_c(t_n - \tau) + \psi(t_n - \tau)^2 + \phi\} \\ \text{env}(t_n, \theta) &= \beta \exp(-\alpha(1 - r \tanh(m(t_n - \tau)))(t_n - \tau)^2) \end{aligned} \quad (9)$$

where $t_n = n\Delta$ is the discrete time samples, and Δ is the sampling interval.

Our objective is to estimate the TOF of the received echo signal, which can be obtained from the signal envelope. In order to reduce the computational burden, the Hilbert transform is employed to extract the signal envelope. To achieve this, it is necessary to define a suitable cost function that

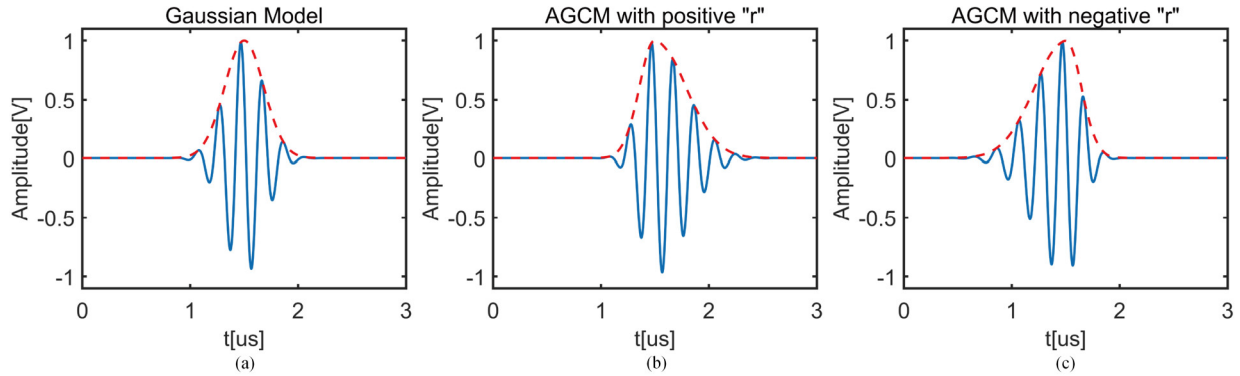


Fig. 1. Comparison of (a) GM and (b) and (c) AGCM with positive “*r*” and negative “*r*”.

minimizes the mean square error between the actual echo parameters and the model echo parameters

$$J(\boldsymbol{\theta}) = \sum_{n=0}^{N-1} (\text{env}(t_n, \boldsymbol{\theta}) - y)^2 \quad (10)$$

where y represents the echo envelope sampled with a sampling frequency above the Nyquist rate.

A. Adaptive Differential Evolution Algorithm

DE, developed by Storn and Price [26], is an evolutionary algorithm inspired by the natural processes of selection and inheritance. The goal is to minimize a fitness function that models the optimization problem with some combined constraints. DE has gained recognition for its simplicity and efficacy, particularly in addressing complex optimization problems. The algorithm iterates continuously through mutation, crossover, and selection to gradually improve and optimize the population and finally find or approach the optimal solution. In practice, if the mutation factor is set too large, the convergence speed of the algorithm becomes slower and the accuracy of the global optimal solution decreases, and if it is too small, the population diversity decreases, so an adaptive operator can be added to make the mutation factor change with the number of iterations to improve the performance of the DE algorithm.

In the DE algorithm, the solutions of the objective function x_1, x_2, \dots, x_n are directly used as individuals $X_{i,G} = (x_1, x_2, \dots, x_n)$, $i = 1, 2, \dots, NP$ in the population. G is the number of evolutions, each individual serves as a candidate solution within the solution space, and the variable dimension D of an individual is equal to the dimension n of the decision variable in the objective function, so $D = n$.

First, for each parameter vector, lower and upper bounds are defined as $X^L < X_{i,G} < X^U$, and initial parameter values are selected in this interval $[X^L, X^U]$. Subsequently, in each generation G , mutation and crossover processes are applied to generate a new population, which contributes to the exploration of the solution space, aiming to identify the desired solutions.

The initial population is generated by a random method as

$$x_j = x_j^L + \text{rand} \cdot (x_j^U - x_j^L), \quad j = 1, 2, \dots, D \quad (11)$$

where rand is the random number between $[0, 1]$, and the population size NP directly affects the convergence speed of the algorithm.

During the mutation process, for a given parameter vector $X_{i,G}$, three vectors are randomly selected from the population and the intermediate individuals obtained after the mutation operation $V_{i,G+1}$ are denoted by

$$V_{i,G+1} = X_{r_1,G} + F \cdot (X_{r_2,G} - X_{r_3,G}) \quad (12)$$

where $r_1, r_2, r_3 \in \{1, 2, \dots, NP\}$, and $r_1 \neq r_2 \neq r_3 \neq i$. $F \in [0, 1]$ is the mutation factor, which is the DE algorithm controlling the magnitude of the difference vector, also known as the scaling factor. The adaptive operator is introduced here as shown in the following equation:

$$\lambda = e^{1 - \frac{Np}{1+Np-G}}. \quad (13)$$

Then, the coefficient of variation F is

$$F = F \cdot 2^\lambda. \quad (14)$$

The crossover was performed by crossing the mutated intermediate individual $V_{i,G+1} = (v_{1i,G+1}, v_{2i,G+1}, \dots, v_{Di,G+1})$ with the target individual $X_{i,G} = (v_{1i,G}, v_{2i,G}, \dots, v_{Di,G})$, as shown in (11). After the crossover, the candidate of the target individual $U_{i,G+1} = (u_{1i,G+1}, u_{2i,G+1}, \dots, u_{Di,G+1})$ is obtained

$$u_{ji,G+1} = \begin{cases} v_{ji,G+1}, & (\text{randb}(j) \leq CR) \text{ or } j = rnbr(i) \\ x_{ji,G}, & \text{others} \end{cases} \quad (15)$$

where $i = 1, 2, \dots, NP$, $j = 1, 2, \dots, D$; $rnbr(i)$ is a random integer in the range of $[1, D]$, $\text{randb}(j) \in [0, 1]$ is a uniformly distributed random number, and the crossover factor $CR \in [0, 1]$ is an important parameter of the algorithm that must be determined by the user and determines the probability that the value of the intermediate individual component replaces the value of the target individual component.

The candidate individuals $U_{i,G+1}$ are evaluated for fitness, and a decision is made whether to replace the current target individual with the candidate individual in the next generation according to (12)

$$X_{i,G+1} = \begin{cases} U_{i,G+1}, & f(U_{i,G+1}) \leq f(X_{i,G}) \\ X_{i,G}, & \text{others} \end{cases} \quad (16)$$

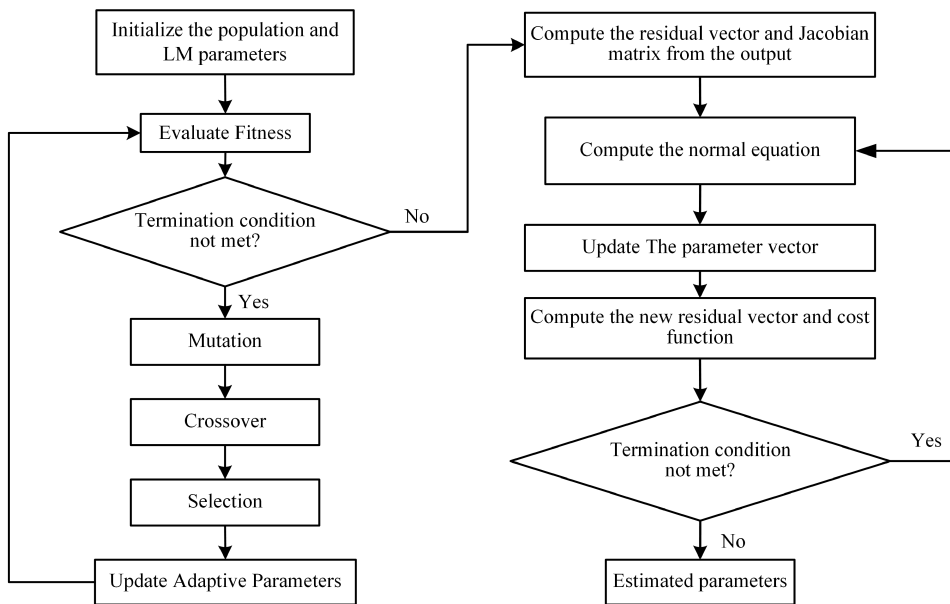


Fig. 2. Flowchart of ADE–LM algorithm.

where f is the fitness function of the optimization problem, and the objective function is generally chosen directly as the fitness function.

For this algorithm, since performing a series of operations (e.g., crossover and mutation) on the individuals in the population will lead to a range of individuals in the population beyond a given range, it is necessary to check and process the boundary conditions for the population obtained after the above operations, as shown in (13)

$$\begin{cases} x^L, & x' < x^L \\ x^U, & x' > x^U \\ x', & \text{others.} \end{cases} \quad (17)$$

B. LM Algorithm

The LM algorithm is an iterative method for finding the minimum of the sum of squares of nonlinear functions and is commonly used in curve fitting, parameter estimation, optimization, and other problems. By combining Gauss–Newton and gradient descent methods in each iteration step, the advantages of both are combined while their disadvantages are avoided [27]. The trade-off between the gradient descent method and the Gauss–Newton method is controlled by introducing a damping factor. When the damping coefficient is larger in the parameter updating process, the gradient descent method is preferred and more stable; when the damping coefficient is smaller, the Gauss–Newton method is preferred and more speed is pursued.

C. ADE–LM Combination Algorithm

While the DE algorithm has demonstrated good performance in approximating the global optimum, it does not guarantee that the final solution is indeed the optimal one. Conversely, the LM algorithm is known for its ability to converge faster and more accurately to the optimal point, given suitable initial values. However, if the initial guess is

far from the global optimum, the LM algorithm may fall into local minima or even divergence. To address these limitations and leverage the strengths of both algorithms, a combined approach is proposed. In the combined algorithm, ADE first runs over a relatively wide range of parameters to obtain the global optimum and then uses these results as the initial guess for the LM algorithm, which can then be used to find the optimal solution quickly. The flowchart of the ADE–LM algorithm is shown in Fig. 2.

Since the result of the ADE execution serves as the initial value of the LM algorithm, the number of iterations of the ADE has a significant impact on the LM algorithm, subsequently, leading to variations in the final results. To investigate this relationship, we set the maximum number of iterations of the LM algorithm to a constant value of 50, while the maximum number of iterations of the ADE algorithm was set to 100–500, respectively, with a step size of 50, and each setting was repeated 1000 times to obtain the statistical data of the ADE–LM method, including the mean, the standard deviation (Std.Dev), and the rate of convergence to the optimal value, which are shown in Table I. The results show that after the number of iterations reaches about 250 times, the output results become relatively stable with minimal fluctuations in the Std.Dev and the ratio of optimal values. Therefore, in the ADE–LM method, the termination condition of the ADE part is defined as reaching 250 iterations or reaching the value of the fitness function less than or equal to $1E - 8$.

The empirical measurement guarantees that the iterative outcomes of the LM algorithm are consistently stable near the maximum allowed iterations. In general, LM could converge quickly; the LM algorithm converged to its minimum within 50 iterations in every one of the 900 described executions, indicating that setting the empirical LM value to 50 is satisfactory. In addition, another cutoff condition for the LM algorithm is that the change in the objective function value is less than $1e - 16$ to ensure accuracy.

TABLE I
ADE-LM ALGORITHM RESULTS FOR DIFFERENT NUMBERS OF ADE ALGORITHM ITERATIONS

	100	150	200	250	300	350	400	450	500
Mean	1.119181	0.225629	0.106028	0.026926	0.025459	0.020101	0.021569	0.022524	0.017166
Std	2.179481	1.040100	0.518611	0.213676	0.208755	0.20684	0.211843	0.198516	0.196421
Optimal ratio	52.1%	90.2	93.6	98.3%	98.4	98.9%	98.8%	98.6%	99.1%

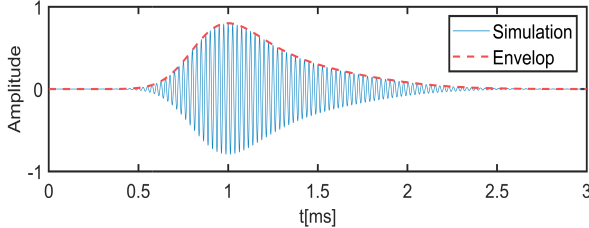


Fig. 3. Simulated signal (blue solid line) and its envelope extraction (red dashed line).

IV. SIMULATION AND EXPERIMENTATION

A. Parameter Settings

In order to test the performance of the asymmetric Gaussian model and the ADE-LM in ultrasonic signal processing, a simulated experiment was set up to simulate the ultrasonic echo signal. The parameters of the model are set as $\theta = [0.8, 10, 0.8, 2, 1]$; therefore, the amplitude $\beta = 0.8$ V, the decay rate (bandwidth factor) $\alpha = 10$ (kHz)², and the arrival time $\tau = 1$ ms. The simulated ultrasonic echo after extracting the envelope using the Hilbert transform is illustrated in Fig. 3.

The following algorithms for estimating the parameters of the envelope are all founded on the parameters of this model.

To ensure a fair comparison, all swarm intelligence algorithms were set to use a consistent population size of 50 with a maximum number of iterations of 500. Furthermore, each algorithm underwent 1000 independent runs to acquire its average numerical performance, and the solution error $f(x) - f(x^*)$ of objective function was collected, where $f(x)$ is the optimum fitness value searched by each algorithm, and $f(x^*)$ is the known fitness of the envelope function. The numerical performance was evaluated using the mean, Std.Dev, and optimal solution ratio of the algorithm's best fitness function value. All algorithms were executed on a PC with 2.80 GHz of GPU and 8 GB of RAM, utilizing the MATLAB 2021b software platform, which functions with a maximum precision of 1E – 323. This means that any value less than 1E – 323 is deemed equal to 0.

B. Ablation Experiment

To verify the effectiveness of the ADE-LM algorithm, we first ran the DE, ADE, and LM algorithms individually, and then combined the DE and ADE with the LM algorithm, respectively, and the experimental results are shown in Table II. After combining the DE algorithm with the adaptive strategy, the performance is significantly improved, but the optimal rate is only 67.4%. Meanwhile, the initial value of the LM algorithm is randomly generated within the upper and lower bounds, so the optimality is reached only in 10.7%

TABLE II
ABLATION EXPERIMENTAL RESULTS

	DE	LM	ADE	DE-LM	ADE-LM
Min	3.91E-04	1.59E-08	1.59E-08	1.59E-08	1.59E-08
Mean	0.015314	10.64950	1.249181	0.180772	0.026926
Std.Dev	0.109721	7.573187	3.376302	0.561064	0.213676
Optimal ratio	0	10.7%	67.4%	89.3%	98.3%

TABLE III
VALUES OF PARAMETERS IN THE COMPARED ALGORITHMS

algorithm	Year	Parameters setting
SO	2022	$c_1 = 0.5, c_2 = 0.05, c_3 = 2, \text{Threshold} = 0.25, 0.6$
DE	1997	$u_F = 0.3, F \sim C(u_F, 0.1), u_{CR} = 0.3, CR = C(u_F, 0.1)$
GWO	2014	Convergence parameter a decreased at interval [0, 2]
PSO	1995	$c_1 = c_2 = 2$, Inertia weight decreased at interval [0.4, 1.2]
SHADE	2013	$u_F = 0.5, F \sim C(u_F, 0.1), CR = C(u_F, 0.1), p=0.2, H=10$
L-SHADE	2014	Same as SHADE parameters except $p = 0.1, NP_{Min} = 4$
ADE-LM		ADE u_F, u_{CR}, F, CR same as DE, $iteration_{max} = 250$ and LM $iteration_{max} = 50$

of the cases. The ADE algorithm has a faster convergence rate in the initial stage of iteration, which makes it able to obtain an approximation that is closer to the optimal solution. When ADE is run in combination with the LM algorithm, the results are significantly better than when it is run alone and in combination with the DE and LM algorithms.

C. Simulation

In this section, we evaluate the numerical performance of the ADE-LM algorithm by comparing it with several variants of the DE algorithm and other state-of-the-art algorithms in the literature, including success-history based parameter adaptation differential evolution (SHADE) [28], L-SHADE [29], Snake Optimizer (SO) [30], Grey Wolf Optimizer (GWO) [31], and PSO [32], with the algorithm's parameter settings as shown in Table III. In addition, we analyze the algorithm's performance in a model that introduces extra noise.

Table IV illustrates that the SHADE, L-SHADE, and ADE-LM algorithms were highly effective in finding optimal envelope parameter values in the majority of the 1000 experiments. Notably, the ADE-LM algorithm achieves a success rate of 98.3% in detecting the optimal solution. In contrast, the DE, GWO, and PSO algorithms are inadequate as they fail to detect the optimal solution. In addition, the ADE-LM algorithm exhibits the smallest Std.Dev among all tested

TABLE IV
COMPARISON WITH OTHER ALGORITHMS USING ACGM

	SO	GWO	PSO	SHADE	L-SHADE	ADE-LM
Mean	2.051	1.406	1.124	0.542	0.519	0.028
Std.Dev	4.009	2.160	2.605	2.312	1.820	0.218
Execution time	2.311	1.761	3.626	5.058	1.306	1.874
Optimal ratio	30.4%	0	0	70.4%	84.8%	98.2%

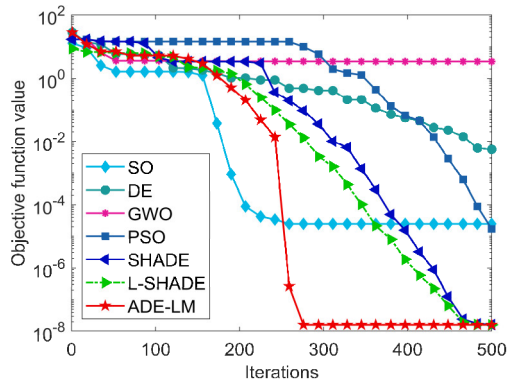


Fig. 4. Comparison of the convergence performance for each algorithm.

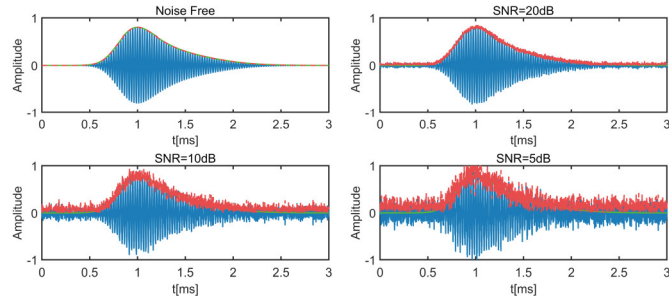


Fig. 5. Envelope extraction of the signal with noise free, 20, 10, and 5 dB, plotted in red dashed line and the original signal envelope plotted in blue solid and green lines.

algorithms and executes slightly slower than L-SHADE and GWO, ranking third in terms of execution time. To enable a more thorough comparison of the algorithms, we analyzed the convergence curves of median error values for SO, DE, GWO, PSO, SHADE, L-SHADE, and ADE-LM, as depicted in Fig. 4. The graph demonstrates that the SHADE, L-SHADE, and ADE-LM algorithms typically identify optimal envelope parameter values in less than 500 iterations. It is noteworthy that the ADE-LM algorithm requires fewer iterations compared with other algorithms. Although the SO algorithm yields acceptable results with fewer iterations, Table IV reveals significant differences in the results. Overall, the ADE-LM algorithm performs well in terms of accuracy, convergence speed, and robustness in the ACGM envelope parameter estimation problem and has obvious advantages over the other six algorithms.

The Gaussian white noise with signal-to-noise ratios of 20, 10, and 5 dB are added to the original signal, respectively, as shown in Fig. 5. From the simulation results, it can be observed that the envelope reconstruction method based on the ACGM is less affected by noise. Moreover, the ADE-LM

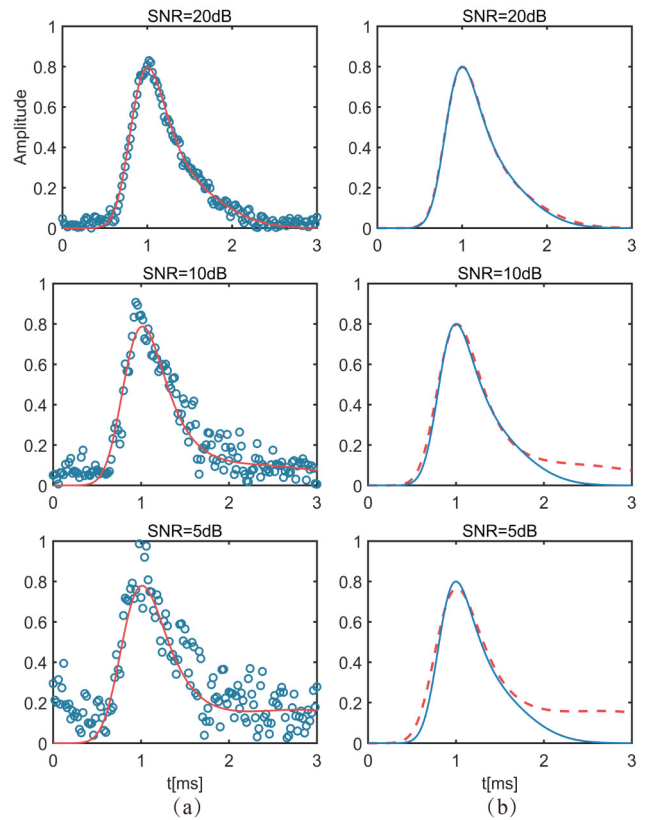


Fig. 6. Fitting result at different signal-to-noise ratios (a) simulated signal envelope sampling point (blue circles) and estimated envelope (red solid line) and (b) simulated (blue solid line) and estimated envelope (red dashed line) under $\text{SNR} = 20, 10$, and 5 dB.

algorithm, which does not require an initial guess, exhibits precise fitting outcomes and rapid convergence. The simulated computational results are presented in Fig. 6.

D. Experiment

The proposed method was utilized to confirm the efficiency of an ultrasonic ranging system in this section. The ultrasonic ranging test system is made up of ultrasonic transmitting and echo receiving circuits, ultrasonic transducer, a digital storage oscilloscope (GWINSTEK MDO-2102EG) for signal acquisition and visualization, a precision displacement platform, and a personal computer, as shown in Fig. 7. The ultrasonic transmission circuit comprises an STM32F429 and a power amplifier (Aigtek ATA-4315). Meanwhile, the echo reception circuit is composed of a preamplifier and filter circuit. This study utilized an AudioWell split piezoelectric transducer to generate ultrasonic waves set at 40 kHz in air at a laboratory temperature of 28.9 °C. The oscilloscope sampling frequency was set at 100 MHz.

To determine the impact of the chosen transducer on the experiment, we conducted a comparative study with other piezoelectric transducers with the same center frequency and bandwidth. The results revealed a variation in the amplitude of the echo signal detected on the oscilloscope, attributable to differences in impedance. However, the ultrasonic transit time measured by different ultrasonic transducers remained

TABLE V
EXPERIMENTAL RESULTS UNDER DIFFERENT DISTANCES

Actual Distance (cm)	Threshold Method		L-SHADE		ADE-LM	
	Distance (cm)	Relative Error (%)	Distance (cm)	Relative error (%)	Distance (cm)	Relative error (%)
1	2.132	113.2%	1.087	8.700%	1.036	3.600%
2	2.941	47.05%	2.003	0.150%	2.003	0.150%
3	3.417	13.90%	3.298	9.933%	3.028	0.933%
4	4.335	8.375%	3.949	1.275%	3.949	1.275%
5	4.862	2.760%	5.137	2.740%	4.996	0.080%
6	5.797	3.383%	5.634	6.100%	5.997	0.050%
7	7.141	2.014%	6.883	1.671%	7.027	0.385%
8	8.534	6.675%	8.271	3.388%	8.008	0.100%
9	9.112	1.244%	8.750	2.778%	8.974	0.289%
10	10.506	5.060%	9.897	1.030%	10.031	0.310%
11	11.441	4.009%	11.059	0.536%	11.036	0.327%
12	12.019	0.158%	11.837	1.358%	12.026	0.217%
13	13.413	3.177%	12.946	0.415%	12.946	0.415%
14	14.399	2.850%	14.160	1.143%	14.036	0.257%
15	15.334	2.227%	14.984	0.107%	14.984	0.107%

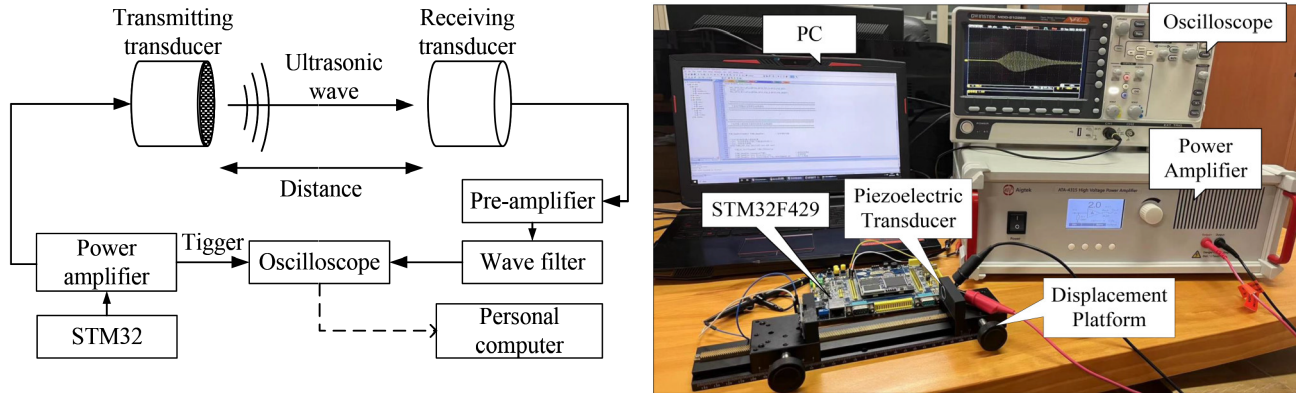


Fig. 7. Ultrasonic ranging measurement system.

constant at a fixed distance. It should be noted that calibration of the start position of the range must be performed according to the specific ultrasonic transducer model due to variations in transducer dimensions.

After the echo signal data points are collected for further processing, the peak arrival time τ of the echo signal is obtained by ACGM reconstruction. However, in the actual ranging, the time from the excitation signal emission to the starting point of the acquired signal echo $t_0 = \tau - t_1$, so the time t_1 between the starting point of the echo signal and the peak should be obtained, as shown in Fig. 8. According to the probability density function of the 1-D Gaussian distribution, the decay rate of the ACGM before the peak is shown by (18), which gives

$$f(x) = \frac{1}{\sqrt{2\pi}\sigma} e^{-\frac{(x-\tau)^2}{2\sigma^2}} \quad (18)$$

$$\sigma = 1/\sqrt{2\alpha} \quad (19)$$

$$\alpha_L = \frac{1}{2\sigma_L^2}, \quad \sigma_L = \frac{1}{\sqrt{\alpha_L(1+r)}}. \quad (20)$$

To ensure the accuracy of the measurement and to compensate for systematic errors, a calibration was performed prior to the measurement. First, the ultrasonic propagation velocity corresponding to the above laboratory temperature values was

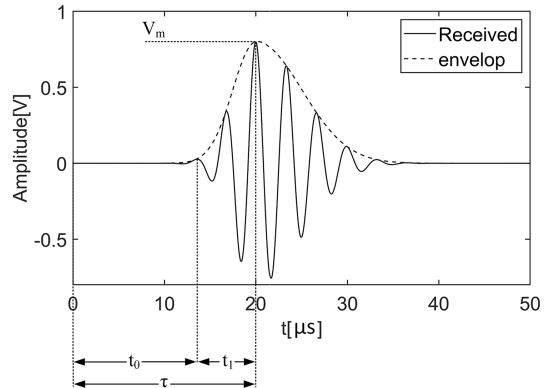


Fig. 8. Principle of ultrasonic ranging measurement.

calculated. Next, a fixed distance was selected and 1000 measurements were taken, with the average of these measurements and the fixed distance difference for each measured distance taken as the calibration constant. To further verify the excellent performance of the ACGM and the ADE-LM algorithm in practical applications, we used the L-SHADE and ADE-LM algorithms to process the collected echo data and compared them with the threshold method. The threshold method is realized by adding a voltage comparator to the echo receiver circuit. Since most of the algorithms were found to perform

poorly relative to the ADE-LM algorithm in the simulation experiments, we selected only the second-ranked L-SHADE algorithm and the ADE-LM algorithm for comparison, and other algorithms were not used for comparison. The measurement results are shown in Table V.

From the experimental results, the accuracy of the parameterized model is significantly better than the threshold method. In addition, compared with the L-SHADE algorithm, the ADE-LM algorithm performs better in the estimation of the optimal solution of the model, and its relative errors are all less than 5%, and even less than 1% in most cases. The thresholding method is susceptible to disturbances that cause the output to be unstable and performs poorly, especially in short-range measurements, so all the results in the table are based on the average of 1000 measurements. On the contrary, the output of the parameterized model is very stable, and the data of multiple measurements are almost consistent, thus ensuring the stability of the estimation results.

V. CONCLUSION

In this article, based on the ACGM, a measurement technique using the echo signal envelope and ADE-LM is proposed. Simulation and experimental results demonstrate that the proposed method outperforms other measurement techniques in terms of accuracy, noise robustness, and output stability. Even under low signal-to-noise ratio conditions, the method maintains high measurement precision. In view of such performance, the TOF measurement technique in this article can be used in distance measurement systems with high accuracy requirements. In this article, five parameters are set for the envelope reconstruction, which are applicable for ultrasonic transducers with different center frequencies. For transducers with the same frequency, the parameter m can be empirically set as a constant to reduce matrix dimension and algorithm execution time. In order to balance accuracy with execution time, the number of matrix dimensions should be chosen based on the ultrasonic TOF estimation application scenario. In addition, the strategy and parameter settings of the algorithm in this article are only for the ACGM, if it is used to solve other problems, the number of iterations and the tolerance of the ADE and LM algorithms should be adjusted according to the actual situation.

REFERENCES

- [1] Z. Lu, C. Yang, D. Qin, Y. Luo, and M. Momayez, "Estimating ultrasonic time-of-flight through echo signal envelope and modified Gauss Newton method," *Measurement*, vol. 94, pp. 355–363, Dec. 2016, doi: [10.1016/j.measurement.2016.08.013](https://doi.org/10.1016/j.measurement.2016.08.013).
- [2] M. Chang, Z. Lu, Q. Huang, and C. Yang, "Parameter estimation for ultrasonic echo signals through improved matching pursuit and flower pollination algorithms," *Measurement*, vol. 194, May 2022, Art. no. 111010, doi: [10.1016/j.measurement.2022.111010](https://doi.org/10.1016/j.measurement.2022.111010).
- [3] W. Wang et al., "Analysis and design of coil-based electromagnetic-induced thermoacoustic for rail internal-flaw inspection," *IEEE Trans. Intell. Transp. Syst.*, vol. 20, no. 7, pp. 2691–2702, Jul. 2019, doi: [10.1109/TITS.2018.2882202](https://doi.org/10.1109/TITS.2018.2882202).
- [4] W. Wang et al., "Novel coil transducer induced thermoacoustic detection of rail internal defects towards intelligent processing," *IEEE Trans. Ind. Electron.*, vol. 71, no. 2, pp. 2100–2111, Feb. 2024, doi: [10.1109/TIE.2023.3250766](https://doi.org/10.1109/TIE.2023.3250766).
- [5] M. M. Saad, C. J. Bleakley, T. Ballal, and S. Dobson, "High-accuracy reference-free ultrasonic location estimation," *IEEE Trans. Instrum. Meas.*, vol. 61, no. 6, pp. 1561–1570, Jun. 2012, doi: [10.1109/TIM.2011.2181911](https://doi.org/10.1109/TIM.2011.2181911).
- [6] L.-B. Mu, K.-J. Xu, B. Liu, L. Tian, and L.-P. Liang, "Echo signal envelope fitting based signal processing methods for ultrasonic gas flow-meter," *ISA Trans.*, vol. 89, pp. 233–244, Jun. 2019, doi: [10.1016/j.isatra.2018.12.035](https://doi.org/10.1016/j.isatra.2018.12.035).
- [7] F. Suñol, D. A. Ochoa, and J. E. Garcia, "High-precision time-of-flight determination algorithm for ultrasonic flow measurement," *IEEE Trans. Instrum. Meas.*, vol. 68, no. 8, pp. 2724–2732, Aug. 2019, doi: [10.1109/TIM.2018.2869263](https://doi.org/10.1109/TIM.2018.2869263).
- [8] J. Ma, K.-J. Xu, Z. Jiang, L. Zhang, and H.-R. Xu, "Applications of digital signal processing methods in TOF calculation of ultrasonic gas flowmeter," *Flow Meas. Instrum.*, vol. 79, Jun. 2021, Art. no. 101932, doi: [10.1016/j.flowmeasinst.2021.101932](https://doi.org/10.1016/j.flowmeasinst.2021.101932).
- [9] W. Wang et al., "MRC-based double figure-of-eight coil sensor system with triple-mode operation capability for biomedical applications," *IEEE Sensors J.*, vol. 21, no. 13, pp. 14491–14502, Jul. 2021, doi: [10.1109/JSEN.2020.3020578](https://doi.org/10.1109/JSEN.2020.3020578).
- [10] W. Wang et al., "Laser-induced surface acoustic wave sensing-based malaria parasite detection and analysis," *IEEE Trans. Instrum. Meas.*, vol. 71, pp. 1–9, 2022, doi: [10.1109/TIM.2021.3124841](https://doi.org/10.1109/TIM.2021.3124841).
- [11] Md. O. Khyam, S. S. Ge, X. Li, and M. R. Pickering, "Highly accurate time-of-flight measurement technique based on phase-correlation for ultrasonic ranging," *IEEE Sensors J.*, vol. 17, no. 2, pp. 434–443, Jan. 2017, doi: [10.1109/JSEN.2016.2631244](https://doi.org/10.1109/JSEN.2016.2631244).
- [12] Z.-J. Yao, Q.-H. Meng, and M. Zeng, "Improvement in the accuracy of estimating the time-of-flight in an ultrasonic ranging system using multiple square-root unscented Kalman filters," *Rev. Sci. Instrum.*, vol. 81, no. 10, Oct. 2010, Art. no. 104901, doi: [10.1063/1.3488057](https://doi.org/10.1063/1.3488057).
- [13] C. H. Han, J. Chung, and S. H. Hong, "Adaptive ultrasonic distance measurement technique for handwriting digitization using reconfigurable analog blocks," *IEEE Trans. Instrum. Meas.*, vol. 59, no. 8, pp. 2240–2242, Aug. 2010, doi: [10.1109/TIM.2010.2047972](https://doi.org/10.1109/TIM.2010.2047972).
- [14] C.-M. Yang, S.-B. Jiang, D.-Y. Lin, F.-M. Lu, Y.-M. Wu, and T.-L. Yeh, "An innovative ultrasonic time-of-flight measurement method using peak time sequences of different frequencies—Part II: Implementation," *IEEE Trans. Instrum. Meas.*, vol. 60, no. 3, pp. 745–757, Mar. 2011, doi: [10.1109/TIM.2010.2063972](https://doi.org/10.1109/TIM.2010.2063972).
- [15] S.-B. Jiang, C.-M. Yang, R.-S. Huang, C.-Y. Fang, and T.-L. Yeh, "An innovative ultrasonic time-of-flight measurement method using peak time sequences of different frequencies: Part I," *IEEE Trans. Instrum. Meas.*, vol. 60, no. 3, pp. 735–744, Mar. 2011, doi: [10.1109/TIM.2010.2063870](https://doi.org/10.1109/TIM.2010.2063870).
- [16] W. Wang, Y. Chen, S. Yang, A. Chan, Y. Wang, and Q. Cao, "Design and experiment of wireless power transfer systems via electromagnetic field near-zone region," *Int. J. Electron.*, vol. 103, no. 10, pp. 1736–1747, Oct. 2016, doi: [10.1080/00207217.2016.1138527](https://doi.org/10.1080/00207217.2016.1138527).
- [17] W. Wang et al., "Wideband gain enhancement of MIMO antenna and its application in FMCW radar sensor integrated with CMOS-based transceiver chip for human respiratory monitoring," *IEEE Trans. Antennas Propag.*, vol. 71, no. 1, pp. 318–329, Jan. 2023, doi: [10.1109/TAP.2022.3222802](https://doi.org/10.1109/TAP.2022.3222802).
- [18] Z. Fang, L. Hu, K. Mao, W. Chen, and X. Fu, "Similarity judgment-based double-threshold method for time-of-flight determination in an ultrasonic gas flowmeter," *IEEE Trans. Instrum. Meas.*, vol. 67, no. 1, pp. 24–32, Jan. 2018, doi: [10.1109/TIM.2017.2757158](https://doi.org/10.1109/TIM.2017.2757158).
- [19] A. K. Sahoo and S. K. Udgata, "A novel ANN-based adaptive ultrasonic measurement system for accurate water level monitoring," *IEEE Trans. Instrum. Meas.*, vol. 69, no. 6, pp. 3359–3369, Jun. 2020, doi: [10.1109/TIM.2019.2939932](https://doi.org/10.1109/TIM.2019.2939932).
- [20] R. Queiros, F. C. Alegria, P. S. Girao, and A. C. C. Serra, "Cross-correlation and sine-fitting techniques for high-resolution ultrasonic ranging," *IEEE Trans. Instrum. Meas.*, vol. 59, no. 12, pp. 3227–3236, Dec. 2010.
- [21] N. Yacef, T. Boudin, and M. Grimes, "Accurate ultrasonic measurement technique for crack sizing using envelope detection and differential evolution," *NDT E Int.*, vol. 102, pp. 161–168, Mar. 2019, doi: [10.1016/j.ndteint.2018.11.018](https://doi.org/10.1016/j.ndteint.2018.11.018).
- [22] H. Hou, D. Zheng, and L. Nie, "Gas ultrasonic flow rate measurement through genetic-ant colony optimization based on the ultrasonic pulse received signal model," *Meas. Sci. Technol.*, vol. 26, no. 4, Apr. 2015, Art. no. 045005, doi: [10.1088/0957-0233/26/4/045005](https://doi.org/10.1088/0957-0233/26/4/045005).

- [23] A. Gholami, F. Honarvar, and H. A. Moghaddam, "Modeling the ultrasonic testing echoes by a combination of particle swarm optimization and Levenberg–Marquardt algorithms," *Meas. Sci. Technol.*, vol. 28, no. 6, Jun. 2017, Art. no. 065001, doi: [10.1088/1361-6501/aa61b6](https://doi.org/10.1088/1361-6501/aa61b6).
- [24] R. Demirli and J. Saniie, "Model-based estimation of ultrasonic echoes. Part I: Analysis and algorithms," *IEEE Trans. Ultrason., Ferroelectr., Freq. Control*, vol. 48, no. 3, pp. 787–802, May 2001, doi: [10.1109/58.920713](https://doi.org/10.1109/58.920713).
- [25] R. Demirli and J. Saniie, "Asymmetric Gaussian Chirplet model for ultrasonic echo analysis," in *Proc. IEEE Int. Ultrason. Symp.*, Oct. 2010, pp. 124–128.
- [26] R. Storn and K. Price, "Differential evolution—A simple and efficient heuristic for global optimization over continuous spaces," *J. Global Optim.*, vol. 11, pp. 341–359, Dec. 1997.
- [27] D. W. Marquardt, "An algorithm for least-squares estimation of nonlinear parameters," *J. Soc. Ind. Appl. Math.*, vol. 11, no. 2, pp. 431–441, Jun. 1963, doi: [10.1137/0111030](https://doi.org/10.1137/0111030).
- [28] R. Tanabe and A. Fukunaga, "Success-history based parameter adaptation for differential evolution," in *Proc. IEEE Congr. Evol. Comput.*, Jun. 2013, pp. 71–78, doi: [10.1109/CEC.2013.6557555](https://doi.org/10.1109/CEC.2013.6557555).
- [29] R. Tanabe and A. S. Fukunaga, "Improving the search performance of SHADE using linear population size reduction," in *Proc. IEEE Congr. Evol. Comput. (CEC)*, Beijing, China, Jul. 2014, pp. 1658–1665, doi: [10.1109/CEC.2014.6900380](https://doi.org/10.1109/CEC.2014.6900380).
- [30] F. A. Hashim and A. G. Hussien, "Snake optimizer: A novel meta-heuristic optimization algorithm," *Knowl.-Based Syst.*, vol. 242, Apr. 2022, Art. no. 108320, doi: [10.1016/j.knosys.2022.108320](https://doi.org/10.1016/j.knosys.2022.108320).
- [31] S. Mirjalili, S. M. Mirjalili, and A. Lewis, "Grey wolf optimizer," *Adv. Eng. Softw.*, vol. 69, pp. 46–61, Mar. 2014, doi: [10.1016/j.advengsoft.2013.12.007](https://doi.org/10.1016/j.advengsoft.2013.12.007).
- [32] J. Kennedy and R. Eberhart, "Particle swarm optimization," in *Proc. Int. Conf. Neural Netw.*, Nov. 1995, pp. 1942–1948.



Jinglin Xiong received the B.Eng. degree from the Henan University of Science and Technology, Luoyang, China, in 2021. He is currently pursuing the M.Eng. degree with the University of Science and Technology Beijing, Beijing, China.

His current research interests include ultrasonic transducers, signal processing, electronic instrumentation, and embedded systems.

Peng Mao received the B.Eng. degree from the Wuhan University of Science and Technology, Wuhan, China, in 2021. He is currently pursuing the M.Eng. degree with the University of Science and Technology Beijing, Beijing, China.

His current research interests include ultrasonic detection, oxygen concentration, electronic instrumentation, and embedded systems.



Xisheng Li received the B.Eng. and Ph.D. degrees from the University of Science and Technology Beijing, Beijing, China, in 1991 and 2000, respectively.

In 1994, he joined the University of Science and Technology Beijing, where he is currently a Professor and a Ph.D. Supervisor. His research interests include advanced sensor technology, weak signal detection, multisensor information fusion, and geomagnetic navigation.